Measurement of spin observables in the quasifree $np \to \{pp\}_s\pi^-$ reaction at 353 MeV

S. Dymov,[1,2,*] V. Shmakova,[2,3] T. Azaryan,[2] S. Barsov,[4] V. Baru,[5,6] P. Benati,[7] D. Chiladze,[3,8] A. Dzyuba,[4] R. Engels,[3] M. Gaisser,[3] R. Gebel,[3] K. Grigoryev,[3,4] P. Goslawski,[9] G. Guidoboni,[7] M. Hartmann,[3] A. Kacharava,[3,†] V. Kamerdzhiev,[3] A. Khoukaz,[9] V. Komarov,[2] P. Kulessa,[10] A. Kulikov,[2] V. Kurbatov,[2] A. Lehrach,[3] P. Lenisa,[7] V. Lensky,[6,11] N. Lomidze,[8] B. Lorentz,[3] G. Macharashvili,[2,8] R. Maier,[3] D. Mchedlishvili,[3,8] S. Merzliakov,[2,3] M. Mielke,[9] M. Mikirtychyants,[3,4] S. Mikirtytchiants,[3,4] M. Nioradze,[8] D. Oellers,[3] H. Ohm,[3] A. Polyanskiy,[6] M. Papenbrock,[9] D. Prasuhn,[3] F. Rathmann,[3] V. Serdyuk,[2,3] H. Seyfarth,[3] E. Steffens,[1] H. J. Stein,[3] H. Stockhorst,[3] H. Ströher,[3] M. Tabidze,[8] S. Trusov,[12] D. Tsirkov,[2] Yu. Uzikov,[2] Yu. Valdau,[3,4] Ch. Weidemann,[3] C. Wilkin,[13] P. Wüstner,[14] Q. J. Ye,[3,15] and M. Zhabitsky[2]

[1]*Physikalisches Institut II, Universität Erlangen-Nürnberg, D-91058 Erlangen, Germany*
[2]*Laboratory of Nuclear Problems, Joint Institute for Nuclear Research, RU-141980 Dubna, Russia*
[3]*Institut für Kernphysik and Jülich Centre for Hadron Physics, Forschungszentrum Jülich, D-52425 Jülich, Germany*
[4]*St. Petersburg Nuclear Physics Institute, RU-188350 Gatchina, Russia*
[5]*Institute of Theoretical Physics, Ruhr-Universität, D-44780 Bochum, Germany*
[6]*Institute for Theoretical and Experimental Physics, RU-117218 Moscow, Russia*
[7]*Università di Ferrara and INFN, IT-44100 Ferrara, Italy*
[8]*High Energy Physics Institute, Tbilisi State University, GE-0186 Tbilisi, Georgia*
[9]*Institut für Kernphysik, Universität Münster, D-48149 Münster, Germany*
[10]*Institute of Nuclear Physics, PL-31342 Cracow, Poland*
[11]*School of Physics and Astronomy, University of Manchester, Manchester M13 9PL, United Kingdom*
[12]*Institut für Kern- und Hadronenphysik, Forschungszentrum Rossendorf, D-01314 Dresden, Germany*
[13]*Physics and Astronomy Department, UCL, Gower Street, London WC1E 6BT, United Kingdom*
[14]*Zentralinstitut für Elektronik, Forschungszentrum Jülich, D-52425 Jülich, Germany*
[15]*Department of Physics and Triangle Universities Nuclear Laboratory, Duke University, Durham, North Carolina 27708, USA*

(Received 12 April 2013; published 8 July 2013)

The transverse spin correlations $A_{x,x}$ and $A_{y,y}$ have been measured in the $\vec{d}\,\vec{p} \to p_{\rm spec}\{pp\}_s\pi^-$ reaction at COSY-ANKE at 353 MeV per nucleon. Here $\{pp\}_s$ denotes a proton-proton pair with low excitation energy, which is dominantly in the $^1S_0$ state. By measuring three protons in the final state it was possible to extract events where there was a spectator proton $p_{\rm spec}$ so that the reaction could be interpreted in terms of quasifree $\vec{n}\,\vec{p} \to \{pp\}_s\pi^-$. The proton and neutron analyzing powers in this reaction were also deduced from this data set by averaging over the polarizations of the deuteron beam and hydrogen target, respectively. The values of A_y were shown to be consistent with a refined analysis of our earlier results obtained with a polarized proton incident on a deuterium target. Taking these data in combination with our previous measurements of the differential cross sections and analyzing powers in the $\vec{p}\,p \to \{pp\}_s\pi^0$ reaction, a more robust partial wave decomposition was achieved. Three different acceptable solutions were found, and the only way of resolving this ambiguity without further theoretical input would be through a measurement of the mixed spin-correlation parameter $A_{x,z}$.

DOI: 10.1103/PhysRevC.88.014001 PACS number(s): 13.75.−n, 14.40.Be, 24.70.+s, 25.40.Qa

I. INTRODUCTION

One of the major challenges in today's physics is to relate the properties of few-nucleon systems and nuclei to the theory of strong interactions, QCD. In this respect there has been significant theoretical progress in establishing an effective field theory that, while having a clear-cut connection to QCD, allows one to study processes involving strongly interacting particles within a well defined perturbative scheme. It is chiral symmetry that provides the preconditions for the construction of an effective field theory, called chiral perturbation theory or simply χPT [1,2].

A modification to the standard χPT approach is necessary when it is applied to pion production in nucleon-nucleon collisions. The large scale, introduced by the initial momentum, has to be considered explicitly [3,4]. Thus, a proper expansion scheme for pion production is now established and a high-precision calculation for the reactions $NN \to NN\pi$ is currently under way [5–8].

One important step forward in our understanding of pion reactions at low energies [9] will be to establish that the same short-range $NN \to NN\pi$ vertex contributes to both p-wave pion production and to low-energy three-nucleon scattering, where a crucial role is played by the identical production operator [10,11]. Apart from pion production and the three-nucleon force, this short-range operator contributes to electroweak processes, such as $pp \to de^+\nu_e$, triton β decay [12–14], and muon absorption on the deuteron $\mu^- d \to nn\nu_\mu$ [15–19], as well as to reactions involving photons, e.g., $\pi d \to \gamma NN$ [13,20] and $\gamma d \to nn\pi^+$ [21,22]. The strength of this production operator cannot be fixed from processes in the one-nucleon sector, such as in pion-nucleon scattering [23].

*s.dymov@fz-juelich.de
†a.kacharava@fz-juelich.de

 ©2013 American Physical Society

The missing term corresponds to an effective $NN \to NN\pi$ vertex, where the pion is in a p wave and both initial and final NN pairs are in relative S waves. It is our aim to extract the relevant partial wave amplitude in pion production from experiment. This is a precondition for a reliable determination of this contact term.

The COSY-ANKE Collaboration has embarked on an ambitious program of performing a complete set of measurements of the $NN \to \{pp\}_s\pi$ reactions at low energy so that a full amplitude analysis can be carried out [24]. By selecting events with excitation energy in the proton-proton system $E_{pp} < 3$ MeV, the resulting diproton $\{pp\}_s$ is overwhelmingly in the $^1S_0$ state. In this case all the possible information on the production amplitudes can be obtained by using polarized beams and targets; no measurements of the polarizations of the final protons are required.

As parts of this program, we have already reported on measurements at $T_p = 353$ MeV of the cross sections $d\sigma/d\Omega$ and proton analyzing powers A_y^p in the $\vec{p}\,p \to \{pp\}_s\pi^0$ reaction [25] and the quasifree $\vec{p}n \to \{pp\}_s\pi^-$ reaction, where a polarized proton beam was incident on a deuterium target [26]. We here complement this information through measurements in inverse kinematics, with a polarized deuteron beam colliding with a polarized hydrogen target. This leads to a determination of the proton-neutron transverse spin correlations $A_{x,x}$ and $A_{y,y}$ in the quasifree $\vec{n}\,\vec{p} \to \{pp\}_s\pi^-$ reaction at the same energy and also an independent measurement of the proton analyzing power for $n\vec{p} \to \{pp\}_s\pi^-$. When this information is used in conjunction with a refined analysis of the earlier data, a more robust amplitude decomposition can be developed for both the $I = 1$ and $I = 0$ channels. The residual ambiguities in this procedure can also be clearly displayed.

The approach to pion production described here was first initiated at TRIUMF through pioneering measurements of the $pn \to \{pp\}_s\pi^-$ differential cross section [27] and the proton analyzing power in the $\vec{p}n \to \{pp\}_s\pi^-$ reaction [28] at 353 MeV, and it was the existence of these data that influenced our choice of beam energy. These results were complemented by TRIUMF data on the quasifree absorption of a π^- on the diproton pair in the ^{3}He nucleus [29]. This provided the shape of the $\pi^-\{pp\}_s \to pn$ cross section but not the normalization.

The group made a partial wave analysis of their results [27] using a methodology developed earlier [30] but their data did not extend over the whole angular region. A more serious drawback was the lack of comparable data on the $pp \to \{pp\}_s\pi^0$ reaction that could be used to constrain the isospin $I = 1$ amplitudes. They therefore ruled out a solution with a large pion d wave, and it was only shortly afterwards that the CELSIUS $pp \to \{pp\}_s\pi^0$ differential cross section measurements were published that showed that there were indeed large pion d-wave contributions, even at relatively low energy [31].

The general amplitude structure for the $NN \to \{pp\}_s\pi$ reaction is discussed in Sec. II, where relations between the amplitudes and the different possible observables are described. Of especial importance are the symmetry relations that link the observables. These relations are, of course, respected by the partial wave development that is also presented here. Since the data reported in this paper were taken quite near threshold, we only keep terms up to and including pion d waves. The experimental apparatus and procedure is the subject of Sec. III. A particular concern here compared to our previous work at ANKE [25,26] is the use of the polarized gas target cell that was required in order to achieve a viable luminosity. Naturally, high and well determined beam and target polarizations are critical in any measurement of a spin correlation but, because the differential cross section had already been measured [26], an absolute normalization was of much lesser importance.

Section IV is devoted to the treatment of the data taken in deuteron-proton collisions with both beam and target being polarized. Unlike the spectator proton in the deuterium target work, that in the $dp \to \{pp\}_s\pi^- p_{\rm spec}$ case is fast and is registered in the forward detector system of the ANKE magnetic spectrometer. Although the principles of the analysis of the two experiments are similar, they differ significantly in their details, especially with respect to the kinematics reconstruction and the handling of the background. The different approaches to the polarimetry are also discussed here. Before the results of the current experiment are presented in Sec. V, we first explain how a reanalysis of the deuterium target data of Ref. [26] was achieved by using fully the timing information provided by the apparatus. This effectively doubled the statistics in the A_y^p measurement. The values achieved here are consistent with the published results and also with those derived from the new polarized hydrogen-target experiment. The latter also led to a consistent shape for the differential cross section. Finally in this section are presented the results on the spin-correlation coefficients. The fact that, on symmetry grounds, $A_{y,y} = 1$ provided an extra check on the product of the beam and target polarizations and led to a more stable evaluation of $A_{x,x}$.

Even after making phase assumptions on the isospin-1 production amplitudes, the partial wave analysis of Sec. VI results in three distinct solutions that have very similar statistical significance. They all reproduce the measured values of the differential cross section, the proton analyzing power, and transverse spin correlation for both $NN \to \{pp\}_s\pi$ reactions. Though one of the solutions might be preferred on theoretical grounds, as stressed in our conclusions of Sec. VII, the ambiguities could only be resolved experimentally through the difficult measurement of the mixed spin-correlation parameter $A_{x,z}$.

II. AMPLITUDES, OBSERVABLES, AND PARTIAL WAVES

A. Polarization observables

In the frame where the z direction is along the beam and the y direction is perpendicular to the reaction plane, the differential cross section for the $pp \to \{pp\}_s\pi^0$ or $np \to \{pp\}_s\pi^-$ reaction takes the form

$$\frac{d\sigma}{d\Omega} = \left(\frac{d\sigma}{d\Omega}\right)_0 \left[1 + P_y A_y^P + Q_y A_y^Q + P_y Q_y A_{y,y} + P_x Q_x A_{x,x} + P_z Q_z A_{z,z} + P_x Q_z A_{x,z} + P_z Q_x A_{z,x}\right], \quad (1)$$

where $\boldsymbol{P}$ and $\boldsymbol{Q}$ are the beam and target polarizations, $(d\sigma/d\Omega)_0$ is the unpolarized cross section, and parity

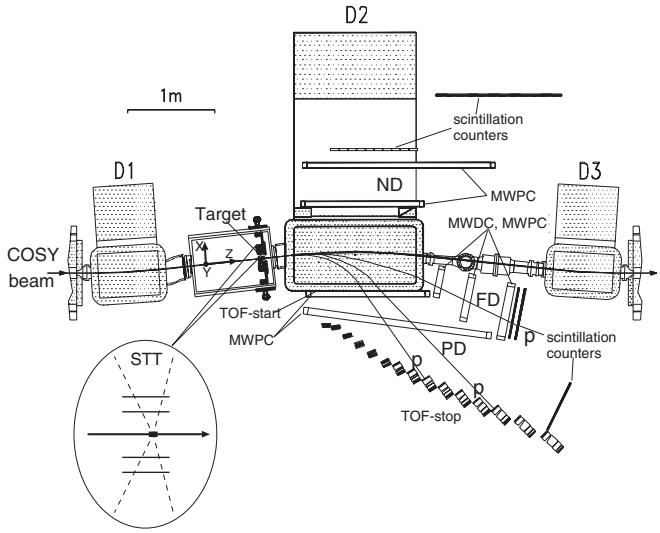

FIG. 1. Top view of the ANKE spectrometer setup, showing the positions of the Positive (PD), Negative (ND), and Forward (FD) detectors, as well as the Silicon Tracking Telescope (STT). The dipoles D1 and D3 deflect the circulating proton beam in and out of the spectrometer, whereas D2 serves as an analyzing magnet. Typical proton trajectories (labeled p) in the FD and PD systems are indicated, as are the axes of the coordinate system at the target.

conservation is assumed. The beam A_y^P and target A_y^Q analyzing powers, as well as the spin-correlation parameters A_{ij}, are all functions of the pion polar angle θ_π.

When, as in this experiment, the beam and target are both polarized perpendicular to the plane of the COSY ring with polarizations P and Q, respectively, it is more convenient to rewrite the expression in the fixed COSY frame as

$$\frac{d\sigma}{d\Omega} = \left(\frac{d\sigma}{d\Omega}\right)_0 \left[1 + \left(P A_y^P + Q A_y^Q\right)\cos\varphi_\pi + P\,Q(A_{y,y}\cos^2\varphi_\pi + A_{x,x}\sin^2\varphi_\pi)\right], \tag{2}$$

where φ_π is the azimuthal angle of the pion in the laboratory reference frame (Fig. 1). We neglect here the small P_z and Q_z components appearing in a quasifree measurement due to the Fermi motion in the deuteron. Their effect is included in the systematic error in the analysis.

B. Production amplitudes and observables

The spin structure of the $pp \to \{pp\}_s\pi^0$ or the $np \to \{pp\}_s\pi^-$ reaction is that of $\frac{1}{2}^+\frac{1}{2}^+ \to 0^+0^-$. Parity and angular momentum conservation then require that the initial nucleon-nucleon pair has spin $S = 1$. There are only two independent scalar amplitudes, A and B, which we define in terms of the full amplitude $\mathcal{M}$ through

$$\mathcal{M} = \boldsymbol{S}\cdot(A\,\hat{\boldsymbol{p}} + B\,\hat{\boldsymbol{k}}), \tag{3}$$

where $\boldsymbol{S}$ is the polarization vector of the initial spin-triplet NN state. $\hat{\boldsymbol{p}}$ and $\hat{\boldsymbol{k}}$ are unit vectors in the center-of-mass (c.m.) frame along the directions of the incident proton and final pion momenta, respectively.

The possible observables are expressed in terms of the amplitudes A and B as

$$\begin{aligned}
\left(\frac{d\sigma}{d\Omega}\right)_0 &= \frac{k}{4p}(|A|^2 + |B|^2 + 2\,\mathrm{Re}[AB^*]\cos\theta_\pi),\\
A_y^P\left(\frac{d\sigma}{d\Omega}\right)_0 &= \frac{k}{4p}(2\,\mathrm{Im}[AB^*]\sin\theta_\pi),\\
A_{x,x}\left(\frac{d\sigma}{d\Omega}\right)_0 &= \frac{k}{4p}(|A|^2 + |B|^2\cos 2\theta_\pi + 2\,\mathrm{Re}[AB^*]\cos\theta_\pi),\\
A_{x,z}\left(\frac{d\sigma}{d\Omega}\right)_0 &= -\frac{k}{4p}(2|B|^2\sin\theta_\pi\cos\theta_\pi + 2\,\mathrm{Re}[AB^*]\sin\theta_\pi),\\
A_y^Q = A_y^P,&\quad A_{y,y} = 1,\quad A_{z,z} = -A_{x,x},\quad A_{z,x} = A_{x,z}.
\end{aligned} \tag{4}$$

The reaction is treated as a quasi-two-body one and, in the evaluation of the phase space factor k/p, the small range of excitation energies in the diproton is neglected.

The observables are not all independent and it is straightforward to show that, for any pion production angle,

$$(A_y)^2 + (A_{x,x})^2 + (A_{x,z})^2 = 1. \tag{5}$$

This means that, if two of the quantities are well measured, there remains only a sign ambiguity in the determination of the third from this quadratic relation.

In addition to the spin dependence of the reaction, there are also two isospin amplitudes $\mathcal{M}^{I=1}$ and $\mathcal{M}^{I=0}$ and, in terms of these, $\mathcal{M}(pp \to \{pp\}_s\pi^0) = \mathcal{M}^{I=1}$ and $\mathcal{M}(np \to \{pp\}_s\pi^-) = (\mathcal{M}^{I=1} + \mathcal{M}^{I=0})/\sqrt{2}$. Since the initial nucleons are in a spin-triplet state, the Pauli principle requires that $\mathcal{M}^{I=1}$ is antisymmetric under the reflection $\boldsymbol{p} \to -\boldsymbol{p}$ whereas $\mathcal{M}^{I=0}$ is symmetric. Due to the presence of the proton momentum factor in Eq. (3), this constraint translates into the requirements that

$$\begin{aligned}
A^{I=1}(\cos\theta_\pi) &= A^{I=1}(-\cos\theta_\pi),\\
B^{I=0}(\cos\theta_\pi) &= B^{I=0}(-\cos\theta_\pi),\\
B^{I=1}(\cos\theta_\pi) &= -B^{I=1}(-\cos\theta_\pi),\\
A^{I=0}(\cos\theta_\pi) &= -A^{I=0}(-\cos\theta_\pi).
\end{aligned} \tag{6}$$

As a consequence of Eq. (6), both $B^{I=1}$ and $A^{I=0}$ vanish at $\theta_\pi = 90^\circ$ and this leads to the important relation at this particular angle,

$$(1 + A_{x,x})\frac{d\sigma}{d\Omega}(np \to \{pp\}_s\pi^-) = \frac{d\sigma}{d\Omega}(pp \to \{pp\}_s\pi^0). \tag{7}$$

Independent of any assumptions made in the subsequent data analysis, the value of the spin correlation $A_{x,x}$ in the $np \to \{pp\}_s\pi^-$ reaction at 90° is fixed completely by the unpolarized $pp \to \{pp\}_s\pi^0$ and $np \to \{pp\}_s\pi^-$ differential cross sections. However, the quasifree nature of the π^- production experiment, as well as the mass differences among both the pions and nucleons, means that there is uncertainty in the relative normalizations of the two unpolarized measurements and so the direct study of $A_{x,x}$ presented in the current work is definitely preferable.

A second useful result for the $pp \to \{pp\}_s \pi^0$ reaction that follows from the symmetry relations of Eq. (6) is that $A_{x,x} = 1$ at 90°.

A complete set of measurements of the observables in Eq. (4) would fix the magnitudes of the amplitudes A and B and their relative phase but the overall phase, which is a function of θ_π is clearly undetermined. Since this phase function can be different for π^0 and π^- production, extra assumptions are required to avoid the consequent ambiguities. These are expressed most clearly in terms of the partial wave amplitudes, to which we now turn.

C. Partial wave decomposition

Our earlier experiments [25,26], and the one reported here, were carried out in the vicinity of 353 MeV and, at such a low beam energy, one may expect that very few pion partial waves will contribute. Keeping terms up to pion d waves, there are three possible transitions from the $I = 1$ initial state, viz., ${}^3P_0 \to {}^1S_0 s$, ${}^3P_2 \to {}^1S_0 d$, and ${}^3F_2 \to {}^1S_0 d$ and we denote the corresponding amplitudes by M_s^P, M_d^P, and M_d^F, respectively. For the $I = 0$ state, there are the two p-wave transitions, ${}^3S_1 \to {}^1S_0 p$ and ${}^3D_1 \to {}^1S_0 p$, whose amplitudes we call M_p^S and M_p^D, respectively.

The scalar amplitudes can be decomposed in terms of these partial waves as

$$\begin{aligned} A^{I=1} &= M_s^P - \tfrac{1}{3} M_d^P + M_d^F \left(\cos^2\theta_\pi - \tfrac{1}{5}\right), \\ B^{I=1} &= \left(M_d^P - \tfrac{2}{5} M_d^F\right) \cos\theta_\pi, \\ A^{I=0} &= M_p^D \cos\theta_\pi, \quad B^{I=0} = M_p^S - \tfrac{1}{3} M_p^D, \end{aligned} \tag{8}$$

which, of course, respect the symmetries shown in Eq. (6).

The partial-wave amplitudes, which depend purely on energy, have a threshold behavior like k^ℓ, where ℓ is the pion angular momentum. However, this power counting is slightly deceptive because it is well known that the s-wave amplitude in pion production is suppressed. As a consequence, it is reasonable for π^0 production to introduce all the terms of Eq. (8) into the expressions for the observables in Eq. (4), since any arising from s-g interference, which have the same threshold dependence as d-d terms, are expected to be very small. This procedure preserves exactly the quadratic relation of Eq. (5). However, our neglect of p-f interference for π^- production may be less justified.

We have already argued [25,26] that, even with a measurement of the complete set of observables in Eq. (4), there are overall phase uncertainties that are functions of θ_π. These are then reflected in ambiguities in the partial wave amplitudes which can only be resolved by making further assumptions. For uncoupled partial waves, provided the inelasticity is very small, the Watson theorem fixes the phase induced by the initial state interaction to that of the elastic nucleon-nucleon scattering [32]. These conditions apply for the ${}^3P_0$ partial wave and so we take $M_s^P = |M_s^P| e^{i\delta_{^3P_0}}$, with $\delta_{^3P_0} = -14.8°$ [33]. The phase associated with the ${}^1S_0$ final pp state is not included because it is common to all partial waves and does not influence the observables.

For coupled channels, such as ${}^3P_2$-${}^3F_2$, the conditions of the Watson theorem do not strictly apply. However, phase shift analysis of pp data at 353 MeV shows that the mixing parameter, as well as the inelasticities, are very small [33]. To a good approximation, we may therefore neglect the coupling and use the Watson theorem also for the individual ${}^3P_2$ and ${}^3F_2$ partial waves, where the phases are $\delta_{^3P_2} = 17.9°$ and $\delta_{^3F_2} \approx 0°$ [33].

Two potential models also suggest that the ${}^3P_2$-${}^3F_2$ channel coupling is weak [34,35]. The quality of this approximation was also checked by explicit calculations of the d-wave production amplitudes within chiral effective field theory up to order m_π/m_N (next-to-next-to-leading order, NNLO) [36]. These show that the phase assumptions made here should be valid to within ±2°. It should, however, be noted that we do not neglect the channel coupling in the ${}^3S_1$-${}^3D_1$ case, where the associated effects can be very strong. The phases of the $I = 0$ amplitudes M_p^S and M_p^D are determined in the fits through their interferences with the $I = 1$ amplitudes.

III. EXPERIMENT

The experiments were carried out with the ANKE magnetic spectrometer installed at an internal beam position of the Cooler Synchrotron (COSY) at the Forschungszentrum Jülich [37]. The ANKE magnetic system comprises three dipole magnets. The spectrometric magnet D2 is used for the momentum analysis of the reaction products while D1 and D3 deflect the circulating beam onto the target and back to the nominal orbit, respectively. The spectrometer contains several groups of detectors that are shown in Fig. 1. The positive side (PD) and forward (FD) [38,39] detectors are used for the fast positively charged ejectiles and the negative side detector (ND) for the negatively charged ones. Each of these groups contains a set of multiwire proportional or drift chambers for track reconstruction and scintillation counters for triggering and measuring the arrival time of the particle.

The program for studying the $NN \to NN\pi$ pion production was started by making measurements of the differential cross section and vector analyzing power with a polarized proton beam incident on unpolarized cluster-jet H_2 and D_2 targets [40]. The deuterium target allowed the $pn \to \{pp\}_s \pi^-$ reaction to be investigated in quasifree kinematics in proton-deuteron collisions. The $pp \to \{pp\}_s \pi^0$ and $pn \to \{pp\}_s \pi^-$ measurements were carried out one after the other, with the same settings of the beam and detectors. This reduced possible systematic uncertainties in the subsequent combined analysis of the data.

To select quasifree kinematic conditions, the momentum of the spectator proton has to be reconstructed for each event. In the proton-deuteron experiment, some of these protons were detected in a silicon tracking telescope (STT) [41] installed in the ANKE target chamber close to the interaction region, as shown in Fig. 1. Since no time information from the STT was used in the original work [26], the main source of background in this analysis was from accidental coincidences between a fast proton pair and a slow spectator proton produced in a separate interaction. In Sec. V A of the present paper we give

the results of a refined analysis of these data that exploits the time information, thus reducing dramatically the accidental background.

The double-polarized measurements reported here were carried out in inverse kinematics, with the polarized deuteron beam incident on the ANKE polarized target [42]. This approach has the advantage that the acceptance of the spectator protons, emitted in the forward direction at about half the beam momentum and detected in the ANKE forward detector (Fig. 1), is significantly higher than in the STT case. This is largely due to the absence of a lower cut on the energy of the spectator proton. It must, however, also be remarked that the ANKE deuterium polarized target had not been commissioned by the time of the current experiment, whereas the hydrogen one had already been tested and successfully used in other experiments. The final diproton pair from the $np \to \{pp\}_s\pi^-$ reaction was recorded in the PD.

Measurements with a polarized deuteron beam and polarized hydrogen target at ANKE have already been described in some detail [43]. In our case, only the vector polarization modes of the beam, with ideal values of $P_\uparrow = \frac{2}{3}$ and $P_\downarrow = -\frac{2}{3}$, were used, but the actual values depend on the precise adjustments of the hyperfine transition units in the source. The polarizations measured at the beginning and end of the experiment at the injection energy of 75.6 MeV with the COSY low-energy polarimeter differed slightly in magnitude from each other, with $P_\uparrow = +61 \pm 4\%$ and $P_\downarrow = -50 \pm 3\%$ for the two modes. The tensor polarization for both modes was estimated to be below 2%. No depolarizing resonances exist for deuterons in the COSY energy range, and so these polarizations should be preserved after acceleration in COSY. However, we cannot guarantee that these results hold throughout the experiment. Accurate polarimetry can only be carried out by using the double-polarization data themselves.

The injected beam was electron cooled and a stacking procedure applied to increase the beam intensity [44]. Typically, ten stacks were made with 30 seconds cooling time for each, resulting in 3–12 $\times 10^9$ deuterons being stored and accelerated. The time loss associated with the stacking was low compared to the total cycle length of 30 minutes. The beam was polarized perpendicularly to the machine plane, and the spin direction reversed every cycle.

In order to increase the target density, the gas from the atomic beam source (ABS) [42] was fed into a Teflon-coated (25 μm thick) aluminum storage cell with dimensions $x \times y \times z = 19 \times 15 \times 390$ mm^3. This resulted in a density of $\sim 10^{13}$ atoms/cm^2 and luminosities of up to $\sim 10^{29}$ cm^{-2}s^{-1}. The ABS produced a jet of atomic hydrogen that was polarized perpendicularly to the COSY beam direction, and the spin orientation of the atoms in the cell was aligned with the vertical field of the D2 dipole. Proton polarizations of above 90% were achieved with the jet [42]. The direction of the spin was reversed every five seconds.

Unlike the measurements with the cluster-jet target, the main source of background with the polarized target was the interactions of the beam particles with the aluminum cell walls. In these interactions, the same processes occur on the nucleons in the nuclei in the cell walls as in the hydrogen. To study the properties of the background, dedicated measurements were conducted with both an empty cell and with nitrogen gas in the cell.

The polarizations of the nucleons in the beam and target were studied using the data on the $\vec{n}p \to d\pi^0$ reaction taken in the $\vec{d}p \to p_{\rm spec}d\pi^0$ process that were recorded simultaneously with those of $np \to \{pp\}_s\pi^-$. In both processes, the spectator proton was detected in the FD (Fig. 1), and this detector was also used for the deuteron formed in the $np \to d\pi^0$ reaction.

In order to study the beam and target polarizations for each spin direction, some data were also taken with an unpolarized beam, an unpolarized target, and both of them unpolarized. For these purposes, the COSY unpolarized beam source was used or the cell was filled from the source of unpolarized H_2 gas.

IV. DATA ANALYSIS IN THE DEUTERON-PROTON EXPERIMENT

A. Reaction selection

The identification of the $np \to \{pp\}_s\pi^-$ reaction starts with the selection of the final diprotons via the time-of-flight (TOF) criterion, as described in Ref. [43]. The difference of the arrival times measured in the scintillation counters of the FD and PD is compared to that calculated under the assumption that the two particles are protons. The spectator proton detected in the FD is then identified by the TOF difference built for it and each of the protons in the diproton. The selection of the final dp pairs from the $dp \to d\pi^0 p_{\rm spec}$ reaction was done analogously. The protons detected in the PD can also be selected using the TOF between the start and stop scintillation counters, shown as TOF-start and TOF-stop in Fig. 1.

The $^1S_0$ events are selected from among the pairs of identified protons by applying a cut on the excitation energy in the pair $E_{pp} < 3$ MeV. This can be done reliably due to the excellent resolution of $\sigma(E_{pp}) < 0.3$ MeV in this E_{pp} region.

It can be seen from the experimental distributions of spectator proton energies $T_{\rm spec}$ in the deuteron rest frame shown in Fig. 2(a) that the acceptance is particularly favorable for

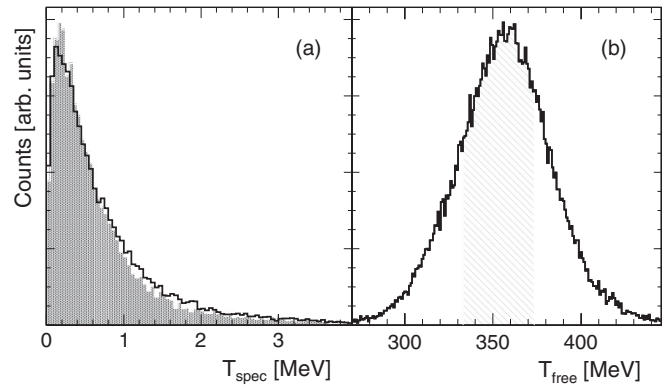

FIG. 2. (a) Experimental (histogram) and simulated (shaded area) distribution in the deuteron rest frame of spectator proton energies from the $dp \to \{pp\}_s\pi^- p_{\rm spec}$ reaction for the selected $T_{\rm free}$ range. (b) Experimental distribution of effective beam energies; the region selected for analysis is shown by the shading.

small $T_{\rm spec}$. The quasifree kinematical conditions are ensured by choosing energies $T_{\rm spec} < 6$ MeV. The value of the spectator proton three-momentum allows one to evaluate the effective beam energy $T_{\rm free}$ in the $np \to \{pp\}_s\pi^-$ reaction,

$$T_{\rm free} = [s - (M_p + M_n)^2]/2M_p, \tag{9}$$

where $\sqrt{s}$ is the total cm energy in the np system and M_p and M_n are the proton and neutron masses. Figure 2(b) shows the experimental distribution of $T_{\rm free}$ and the region of $T_{\rm free} = (353 \pm 20)$ MeV that is retained in the analysis.

After application of the selections described above, the $np \to \{pp\}_s\pi^-$ and $np \to d\pi^0$ reactions could be identified by comparing the missing-mass peaks in the data with the masses of the missing pions.

B. Background subtraction

The main source of background consisted of events corresponding to the reactions studied, but produced on the nucleons of the aluminum in the cell walls. The only difference between good dp data and background was in the shape of the missing-mass distributions. Due to the Fermi smearing in the aluminum, these were significantly wider for the background. Dedicated measurements with the empty cell and filled with nitrogen (N_2) gas were carried out to derive the shape of the background. Although more accurate background distributions could be obtained through measurements with the empty cell, it was realized that collecting the necessary statistics would require too much time. The N_2 target, which produced a signal similar to that from aluminum, led to substantially higher statistics.

Figure 3 shows the missing-mass spectra for the $np \to \{pp\}_s\pi^-$ and $np \to d\pi^0$ reactions obtained with the hydrogen cell target. Each spectrum was fitted by the sum of a Gaussian and a scaled distribution of the background collected with N_2 in the cell. The shape of the background was determined separately for all the bins in the polar and azimuthal angles used in the analysis.

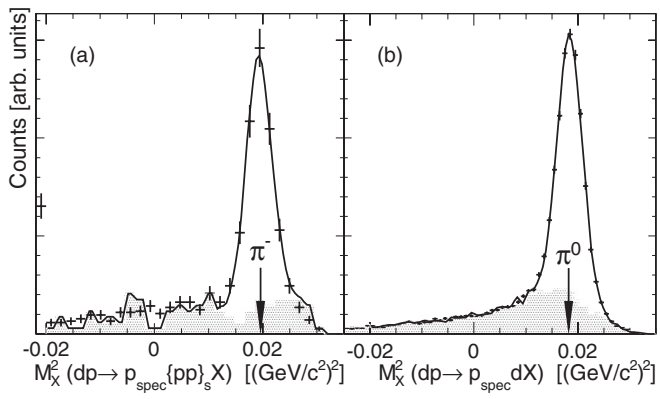

FIG. 3. Missing-mass squared for the (a) $dp \to p_{\rm spec}\{pp\}_s X$ and (b) $dp \to dpX$ reactions. The data with error bars were obtained with hydrogen in the cell. The shaded area shows the scaled background and the line the total fitted function.

C. Reconstruction of the kinematics

The reconstruction of the momentum of a particle passing through the analyzing magnet D2 relies on the information on the position of the interaction vertex. In the case of a storage cell, this is known much less precisely than for the pointlike cluster-jet target. Uncertainties in the interaction vertex location lead to poorer resolution for the momentum of the detected particle, as well as to systematic deviations in its value. To alleviate this problem, a vertex reconstruction procedure was applied that fits simultaneously the trajectories of the particles and their arrival times. The parameters of the fit are the three-momenta of the particles and the longitudinal coordinate Z of the vertex. The accuracy achieved in the coordinate was $\sigma(Z) = 5.6$ cm for the $dp \to pp\pi^- p_{\rm spec}$ process and $\sigma(Z) = 12$ cm for $dp \to d\pi^0 p_{\rm spec}$. Knowing Z even with such a limited precision allows one to reject interactions with the unpolarized gas in the target vacuum chamber outside of the cell. The resulting polar and azimuthal angular resolutions achieved for both the $np \to \{pp\}_s\pi^-$ and $np \to d\pi^0$ reactions were in the $\sigma(\vartheta_\pi) = 2^\circ$–$6^\circ$ and $\sigma(\varphi_\pi) = 4^\circ$–$10^\circ$ ranges, depending on the angular regions. The resolution in spectator energy was better than 0.15 MeV and that in effective beam energy about 4 MeV.

D. Relative normalization. Polarimetry

In order to extract values of the polarization observables, one has to know the ratios of the integrated luminosities for each of the beam and target spin orientations. This could be done straightforwardly if the experiment involved only single-polarized data by comparing the numbers of counts in kinematical regions where the analyzing power vanishes, such as in the forward direction for the $np \to d\pi^0$ reaction. Using the vector analyzing power available at 353 MeV for the $\vec{p}p \to d\pi^+$ reaction from the SAID database [45], one could then determine either the beam or target polarization. The asymmetry of counts for each spin direction with respect to the properly normalized unpolarized counts yields the polarizations for each direction separately. The results obtained from a limited sample of single-polarized data for the target (proton) polarization were $Q_\uparrow = 59 \pm 7\%$ and $Q_\downarrow = -70 \pm 11\%$. Those for the beam (neutron) were $P_\uparrow = 55 \pm 8\%$ and $P_\downarrow = -45 \pm 8\%$. Within the large error bars the two sets of magnitudes are consistent and only a very small error is introduced by assuming this equality in the subsequent analysis.

It is perhaps comforting that the neutron beam polarizations obtained here are both consistent with a factor of 0.9 times the deuteron vector polarizations measured at injection at the beginning and end of the experiment. Furthermore, the differences in the magnitudes of the polarizations with spin up or down are relatively small. However, both the beam and target polarization results given here are merely indicative; it is absolutely necessary to deduce their averages over the course of the experiment and this means extracting the averages from the double-polarized data. This also has the advantage that much larger statistics are then available.

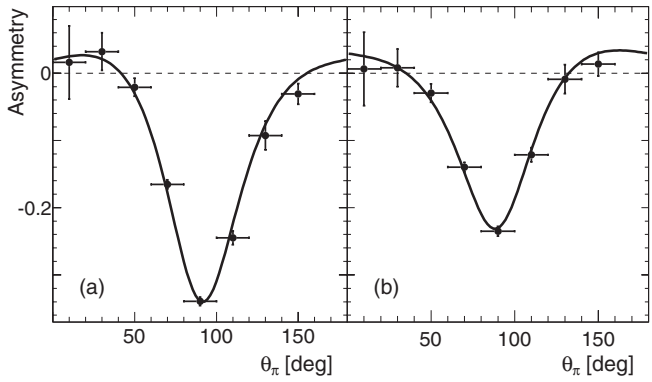

FIG. 4. Experimental asymmetry in the quasifree $\vec{n}p \to d\pi^0$ data for (a) the target polarization and (b) the beam polarization. The curves show the SAID predictions for A_y in $\vec{p}p \to d\pi^+$ at 353 MeV [45], scaled with the value of polarization to fit the data, which are shown with their statistical errors.

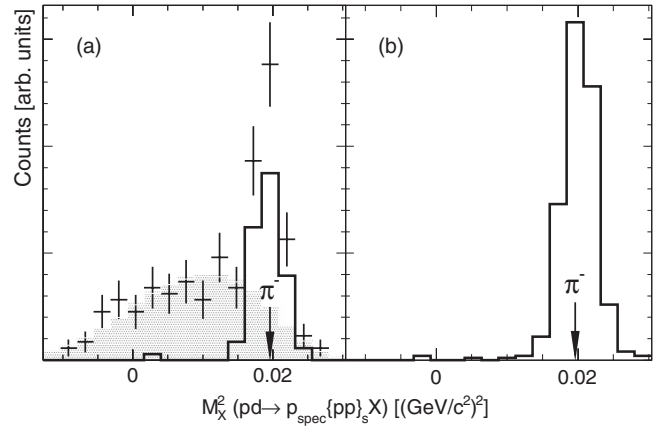

FIG. 5. The experimental $pd \to p_{\rm spec}\{pp\}_s X$ missing-mass-squared spectrum. (a) Spectrum measured using the first two STT layers without the time criterion (points with error bars) and the constructed and scaled background (filled area) [26]. The data obtained using the time criterion (line) show almost no background. (b) Spectrum for the same angular bin and detector combination obtained from the first STT layer only by using the timing information.

As can be seen from Eq. (2), in this double-polarized case the polarization effects in the $\vec{n}\vec{p} \to d\pi^0$ cross section do not disappear in the forward direction and, to exploit such data for polarimetry purposes, one has to know the spin-correlation coefficients for the reaction as well as the analyzing power. Under our experimental conditions, in a first approximation, the integrated luminosities can be assumed to be equal so that one can sum the beam polarization modes to define polarization of the target and vice versa. Using the transverse spin-correlation coefficients for $\vec{p}\vec{p} \to d\pi^+$ at 353 MeV [45], values of the polarizations could be deduced, and these led to the following estimates for the luminosity ratios: $R_{\uparrow\downarrow} = L_{\uparrow\downarrow}/L_{\uparrow\uparrow} = 0.97 \pm 0.02$, $R_{\downarrow\uparrow} = L_{\downarrow\uparrow}/L_{\uparrow\uparrow} = 0.95 \pm 0.02$ and $R_{\downarrow\downarrow} = L_{\downarrow\downarrow}/L_{\uparrow\uparrow} = 1.05 \pm 0.02$, $R_{\uparrow\uparrow} \equiv 1$.

Although the luminosity ratios are, as expected, close to unity, the deviations from this are important in the extraction of the polarizations. Inserting these into the analysis, the mean magnitudes of the beam and target polarizations were found to be $|P| = 50\% \pm 3\%(\text{stat}) \pm 3.5\%(\text{syst})$ and $|Q| = 69\% \pm 2\%(\text{stat}) \pm 3.5\%(\text{syst})$. The 3.5% systematic errors arise from uncertainties in the $\vec{p}\,\vec{p} \to d\pi^+$ calibration reaction [45]. These results are illustrated in Fig. 4, where the experimental asymmetries in the $\vec{n}p \to d\pi^0$ counts are fitted by the scaled analyzing power for the $\vec{p}p \to d\pi^+$ reaction. We should stress that here and elsewhere in the paper we take θ_π to be the c.m. angle of the pion with respect to the incident proton direction, as we did for our deuterium target data [26].

It should be noted that, since the spin-correlation parameter $A_{y,y}$ for the $\vec{p}n \to \{pp\}_s\pi^-$ reaction is constrained to be unity, the product PQ of the polarizations can be independently determined from an analysis of the reaction data themselves.

V. RESULTS

A. Reanalysis of the proton beam data

In Ref. [26] we presented results from measurements of the unpolarized differential cross section and proton analyzing power of the $\vec{p}n \to \{pp\}_s\pi^-$ reaction with the polarized proton beam and a deuterium cluster-jet target. The spectator protons were here detected in one of the silicon tracking telescopes that were installed in the ANKE target chamber (Fig. 1). Each STT, located to the left and right of the beam, contained two layers of silicon strip detector. Only protons passing through the first layer and stopping in the second were analyzed, and this limited the energy of the slow spectator proton to be in the range $2.6 < T_{\rm spec} < 6$ MeV. The energy loss in the two layers allowed one to separate protons from deuterons [46], while the two-dimensional coordinates measured in each layer enabled the reconstruction of the direction vector and the coordinates of the interaction point. The latter was used to help in the background suppression.

The major source of background in this approach was accidental coincidences with a random spectator proton in the STT. The background level in the pion peak of the $pn \to \{pp\}_s\pi^-$ data was up to 50% and a special procedure had to be derived in order to evaluate its shape in the missing-mass spectra [26]. A way to access the time information from the STT has recently been established, and this has allowed the deuterium target data to be reanalyzed with a substantially lower background, as demonstrated by the results shown in Fig. 5(a).

Suppressing the accidental background also allowed one to increase the statistics by considering also the slower spectator protons that stopped in the first layer of the STT. This was possible because, at a beam energy of 353 MeV, the $pd \to ppp\pi^-$ reaction is the only process that can result in three positively charged hadrons in the final state. One can therefore identify the reaction, merely by making a missing-mass selection, without explicitly identifying the spectator proton through its energy loss. The second layer of the STT served as a veto for such events. The center of the beam-target interaction region was used as the starting point on the track that defined the direction of the momentum vector. Although the accuracy of the measurement of the spectator three-momentum was poorer in this case, it was still

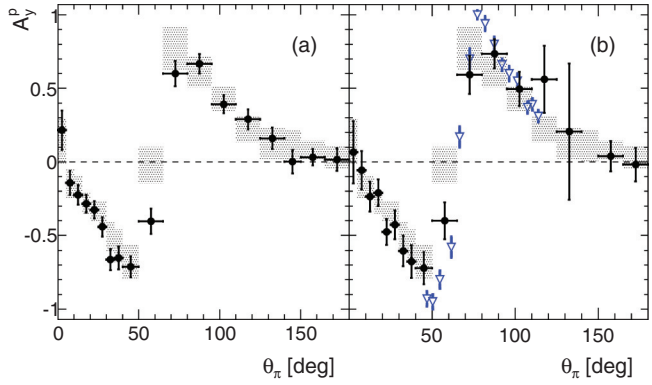

FIG. 6. (Color online) Analyzing power A_y^p for the quasifree $\vec{p}n \to \{pp\}_s\pi^-$ reaction at 353 MeV with the $E_{pp} < 3$ MeV cut. The published ANKE data [26] are shown with the shaded error bands. The black circles show the reanalyzed ANKE data with statistical errors using E_{pp} cuts of (a) 3 MeV and (b) 1.5 MeV. The TRIUMF data [27] are represented by the blue triangles.

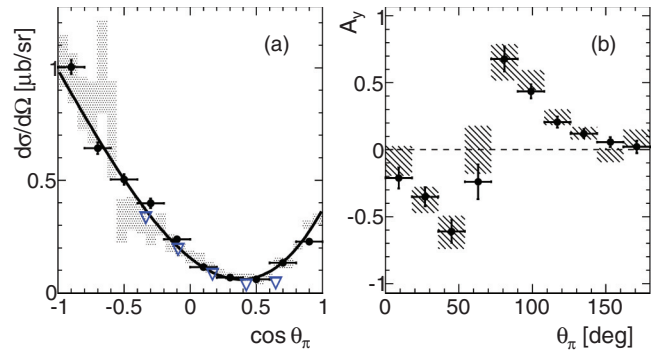

FIG. 7. (Color online) Observables measured for the $pn \to \{pp\}_s\pi^-$ reaction at 353 MeV using the $E_{pp} < 3$ MeV cut. (a) The unpolarized differential cross section. The published ANKE data [26] are shown by the shaded error bands and the curve is a direct cubic fit to these data. The black circles show the data with statistical errors obtained in the new ANKE double-polarized experiment. Since no absolute normalization was here achieved, these values were scaled by an arbitrary overall factor. The TRIUMF data [28] are shown by the blue triangles. (b) The proton analyzing power A_y^p (points) and neutron analyzing power A_y^n (shaded bands) obtained simultaneously in the double-polarized experiment.

quite sufficient for the identification of the $pn \to \{pp\}_s\pi^-$ reaction by calculating the mass of the missing pion. Without exploiting the time information, the level of background for such events would made this sample practically unusable. After application of this criterion the background was reduced to the few-percent level, as shown in Fig. 5(b). However, since the overall acceptance is much harder to estimate for these events, they were only used to improve the measurement of the analyzing power. This approach increased the statistics for $\theta_\pi > 30^\circ$ by about a factor of 2. The improvement was far less significant at smaller angles, where the pions were directly measured in the negative side detector.

The enhanced background suppression and improved spectator proton energy range led also to a better determination of the beam polarization. The relative polarization uncertainty of 11% introduced the largest systematic error in the combined amplitude analysis of the $pp \to \{pp\}_s\pi^0$ and $pn \to \{pp\}_s\pi^-$ reactions [26]. The new value of the beam polarization of 63.3 ± 3.6 %, where the error is dominated by that of the calibration data [45], reduces this uncertainty by a factor of 2.

The increased statistics allowed us to test the effect of imposing the tighter limitation on the diproton excitation energy, $E_{pp} < 1.5$ MeV, that was used at TRIUMF [27]. Figure 6 shows the newly obtained A_y^p data for the two E_{pp} cuts compared with the published ANKE and the TRIUMF data. It is seen that the analyzing powers are little changed through the introduction of the harder E_{pp} cut that was used for the TRIUMF data [27].

B. Extraction of the unpolarized cross section and analyzing power from double-polarized data

The study of the $\vec{n}\,\vec{p} \to \{pp\}_s\pi^-$ reaction in dp kinematics, and with a different set of detectors, opens the possibility of checking the systematic uncertainties in the published ANKE data on $d\sigma/d\Omega$ and A_y^p [26], as well as the consistency of the more complicated analysis of the double polarization measurements with the long cell target. The overall statistics collected in the two experiments are similar but, due to the difference in acceptance, the angular distributions of raw events differ significantly.

It is much harder to evaluate a precise value for the absolute normalization for data taken with a long cell target than it is for a pointlike vertex experiment. We therefore present in Fig. 7(a) only an arbitrarily scaled cross section obtained from the cell data to facilitate a comparison of its shape with the published results from ANKE [26] and TRIUMF [28]. There is reasonable consistency between the two ANKE experiments, in particular in the forward pion angle region where the TRIUMF data begin to deviate.

The proton and neutron analyzing powers were extracted from the double-polarized data by averaging over the beam and target polarization states, respectively. Although the polarization of the beam neutron is less than that of the target proton, and so the error bars are larger, the values of A_y^p and A_y^n shown in Fig. 7(b) are mutually compatible. This provides extra evidence to support the validity of the current experiment and its analysis. The new results, which are completely consistent with the published ANKE data, have comparable statistical and systematic uncertainties and so can be used in a combined analysis.

C. Measurement of the spin-correlation coefficients $A_{x,x}$ and $A_{y,y}$

It follows from Eq. (2) that the experimental double-polarized asymmetry ξ can be written as

$$\xi = \frac{\Sigma_1 - \Sigma_2}{\Sigma_2 + \Sigma_2}, \quad \frac{\xi}{PQ} = A_{x,x}\sin^2\varphi_\pi + A_{y,y}\cos^2\varphi_\pi, \quad (10)$$

where $\Sigma_1 = N_{\uparrow\uparrow} + N_{\downarrow\downarrow}$ and $\Sigma_2 = N_{\uparrow\downarrow} + N_{\downarrow\uparrow}$. Here N represents the number of events collected with the directions of the

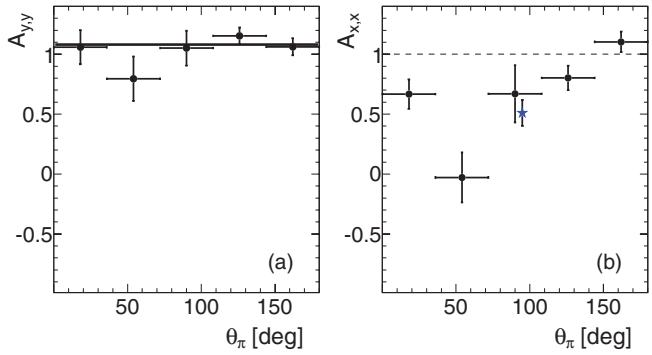

FIG. 8. (Color online) Spin-correlation coefficients for the $\vec{n}\,\vec{p} \to \{pp\}_s\pi^-$ reaction at 353 MeV with statistical errors as a function of the pion emission angle. (a) $A_{y,y}$. The horizontal line represents a fit with a constant value. (b) The values of $A_{x,x}$ were subsequently deduced by demanding that $A_{y,y} = 1$ for all pion angles. The systematic uncertainties of the 90° point (blue star, shifted for visibility) deduced from Eq. (7) are much larger than the purely statistical errors shown.

beam and target spins indicated by the arrows, normalized to the corresponding relative luminosity R, defined in Sec. IV D. PQ is the product of the beam and target polarizations.

The background was subtracted separately from the combinations $\Sigma_1 - \Sigma_2$ and $\Sigma_1 + \Sigma_2$. Since the background contribution showed practically no polarization dependence, its effects were very small in the difference.

The experimental data were divided into five bins in the pion emission angle θ_π and ξ/PQ was fitted as a linear function of $\cos^2\varphi_\pi$ in each bin. The acceptance of the apparatus was significantly higher for events with large $\cos^2\varphi_\pi$ so that the value of $A_{y,y}$ was determined with smaller uncertainty than that of $A_{x,x}$. The results for both spin-correlation parameters are shown in Fig. 8 as a function of θ_π.

As can be seen from Eq. (10), the experiment is essentially self-analyzing. The values obtained for $A_{x,x}$ and $A_{y,y}$ depend only on the product of the beam and target polarizations PQ and this can be determined by requiring that $A_{y,y} = 1$ when averaged over all pion angles. This property of the experiment also provides a powerful tool to study systematic uncertainties in the measurement. The fitted constant value of $A_{y,y} = 1.08 \pm 0.04$ is consistent with unity when one takes into account the 0.11 uncertainty coming from the error in the polarization product. By demanding that $A_{y,y} = 1$, one obtains the more precise measurement of the polarization product, $PQ = 0.373 \pm 0.015$, that can then be used in the determination of $A_{x,x}$.

In order to reduce the uncertainty in the extraction of $A_{x,x}$, it was assumed that $A_{y,y} = 1$ for all θ_π and the $\cos^2\varphi_\pi$ fit repeated. It was this procedure that led to the results shown in Fig. 8(b). The uncertainty in $A_{x,x}$ is dominated by statistics. The systematic uncertainties originated from (i) the polarization product error (0.04), (ii) the possible difference in the up/down polarizations (0.01), (iii) the relative normalization uncertainty (0.023), and (iv) the effect of a longitudinal spin component arising from the Fermi motion in the deuteron (up to 0.07).

Also shown in Fig. 8(b) is the value at 90° of $A_{x,x} = 0.51 \pm 0.11$ that is deduced from Eq. (7) by using direct fits to the π^0 and π^- production cross sections. However, the error bar quoted here is purely statistical and does not include the systematic effect from the uncertainty in the relative normalizations.

VI. PARTIAL WAVE ANALYSIS

The partial wave fitting of Ref. [26], described in detail in Sec. II C, was repeated taking into account the new data presented here. These include the reanalyzed A_y^p from the deuterium cluster-jet experiment, the newly estimated A_y^p from the hydrogen cell data, and the $A_{x,x}$ results. The values of the unpolarized $(d\sigma/d\Omega)_0$, for both π^0 and π^- production, and the A_y^p for π^0 production were taken from our previous work [25,26].

In contrast to the procedure adopted in Ref. [26], the squares of pion d-wave amplitudes were not neglected in the analysis. In addition, effects from the uncertainties in the data normalization were included by constructing the full nondiagonal covariance matrix $\mathcal{M}$ for the measured data points and minimizing the general form $\chi^2 = \delta_i \mathcal{M}_{ij}^{-1} \delta_j$, where δ_i is the ith data-point residual.

A grid search for χ^2 minima was performed in the space of the magnitudes and phases of the p-wave amplitudes, with the s- and d-wave amplitudes being fixed by the fit to the π^0 data. The search revealed three minima with very similar values of χ^2. The five amplitudes were then fitted in the vicinity of each minimum. The properties of the three solutions are listed in Table I, where the first minimum corresponds to that found

TABLE I. Values of the real and imaginary parts of the amplitudes for five lowest partial waves deduced from fits to the ANKE $pp \to \{pp\}_s\pi^0$ and $np \to \{pp\}_s\pi^-$ measurements at 353 MeV. Also shown are the ratios of the imaginary to real parts of the amplitudes that have been freely fitted. The other three ratios are fixed by the Watson theorem.

Amplitude	Real	Imaginary	Im/Re
	Solution 1: $\chi^2/\text{ndf} = 101/82$		
M_s^P	53.4 ± 1.0	-14.1 ± 0.3	
M_d^P	-25.9 ± 1.4	-8.4 ± 0.4	
M_d^F	-1.5 ± 2.3	0.0 ± 0.0	
M_p^S	-37.5 ± 1.7	16.5 ± 1.9	-0.44 ± 0.06
M_p^D	-93.1 ± 6.5	122.7 ± 4.4	-1.32 ± 0.11
	Solution 2: $\chi^2/\text{ndf} = 103/82$		
M_s^P	52.7 ± 1.0	-13.9 ± 0.3	
M_d^P	-28.9 ± 1.6	-9.4 ± 0.5	
M_d^F	3.4 ± 2.6	0.0 ± 0.0	
M_p^S	-63.7 ± 2.5	-1.3 ± 1.6	0.02 ± 0.03
M_p^D	-109.9 ± 4.2	52.9 ± 3.2	-0.48 ± 0.03
	Solution 3: $\chi^2/\text{ndf} = 106/82$		
M_s^P	50.9 ± 1.1	-13.4 ± 0.3	
M_d^P	-26.3 ± 1.5	-8.5 ± 0.5	
M_d^F	2.0 ± 2.5	0.0 ± 0.0	
M_p^S	-25.4 ± 1.9	-7.3 ± 1.5	0.20 ± 0.07
M_p^D	-172.2 ± 5.6	92.0 ± 6.2	-0.53 ± 0.04

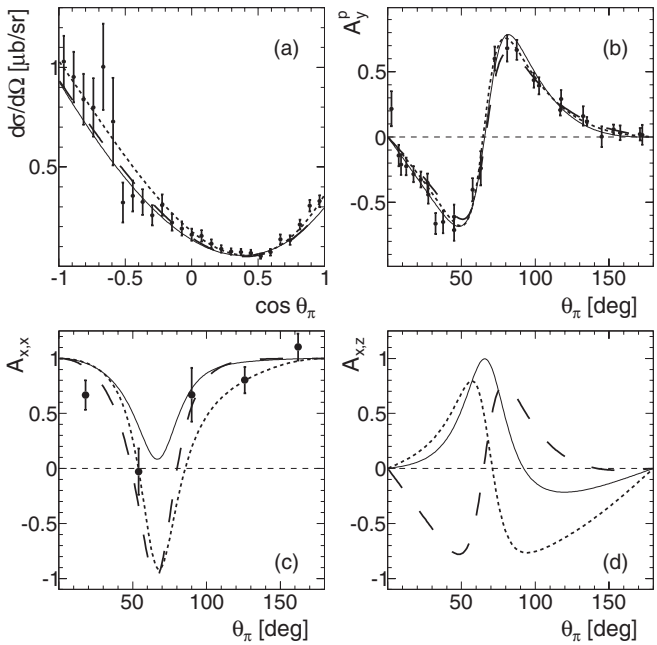

FIG. 9. Predictions of the partial wave analysis for the $pn \to \{pp\}_s\pi^-$ reaction at 353 MeV with the $E_{pp} < 3$ MeV cut. Also shown are the ANKE experimental data with statistical errors. The full, long-dashed, and short-dashed lines correspond to solutions 1, 2, and 3, respectively, as noted in Table I. (a) Differential cross-section taken from Ref. [26], (b) A_y^p data from this work, (c) $A_{x,x}$ data from this work, and (d) $A_{x,z}$, for which there are yet no experimental data.

in Ref. [26]. The solutions differ mostly in the parameters of the p-wave amplitudes, while the s and d waves stay essentially unchanged. The existence of alternative solutions is not entirely unexpected and some of their properties were studied both theoretically [47] and empirically [30], though neither of these works considered the case where some of the phases are fixed by the Watson theorem.

Figure 9 shows the predictions for the $np \to \{pp\}_s\pi^-$ observables for the three solutions detailed in Table I compared with the ANKE data. The solutions describe equally well the cross section and A_y^p data, but differ significantly in $A_{x,x}$, and especially in $A_{x,z}$. The $A_{x,x}$ data presented in this work follow the gross features of all three predictions. However, while favoring somewhat solutions 2 and 3, this is not decisive given the statistical uncertainties. In view of the drastically different predictions for $A_{x,z}$, a measurement of this coefficient becomes especially important for resolving the ambiguities in the analysis and determining which of the three possible solutions is the physical one.

VII. CONCLUSIONS

We have studied the $np \to \{pp\}_s\pi^-$ reaction in the vicinity of 353 MeV per nucleon using a polarized deuteron beam incident on a polarized hydrogen target cell. Although the primary aim was the measurement of the transverse spin-correlation coefficient $A_{x,x}$, the proton analyzing power A_y^p was also determined by averaging over the deuteron beam polarizations. The consistency of these latter results with those obtained earlier with a proton beam [26] suggests that many systematic effects are indeed under control. This belief is reinforced by the values of the differential cross section that were extracted from the new double-polarized data. Although the luminosity could not be reliably evaluated for these data, the shape of the cross section agreed well with our published data [26] and, in particular, showed the small forward-angle peak that was absent from the TRIUMF pion-production results [28], though there are indications of it in their pion absorption data [29].

In the earlier experiment [26] the spectator protons were detected in the silicon tracking telescopes and, in order to control the background, only spectators that had sufficient energy to pass completely through the first silicon wafer were accepted. However, with increased understanding of the detector timing information, in a reanalysis of the old data, events have been retained where the proton stopped in the first STT layer. These stopping events give results that are consistent with those of the previous set and the reanalysis has doubled the A_y^p statistics. These events have also allowed us to investigate the effect of making a tighter selection on the diproton excitation energy. Taking a cut at 1.5 MeV, as used at TRIUMF [27], gives very similar A_y^p results to our original 3 MeV cut.

The combined $pp \to \{pp\}_s\pi^0$ and $np \to \{pp\}_s\pi^-$ data sets have been used in the partial wave analysis presented here and no attempt has been made to include any effects associated with the breaking of isospin invariance. For example, although $\delta_{^3P_0}$ is suggested to be -14.8° in pp elastic scattering, the corresponding figure in the np case is -16.7° [33]. There are also effects that must arise from the pion mass differences and this is one reason for insisting on a direct measurement of $A_{x,x}$ rather than trying to deduce its value from independent measurements of the $pp \to \{pp\}_s\pi^0$ and $np \to \{pp\}_s\pi^-$ differential cross sections and relying on Eq. (7).

We can see from Fig. 9 that the three partial wave solutions of Table I can all describe reasonably well the measured values of the differential cross section, the analyzing power, and the transverse spin correlation in the $np \to \{pp\}_s\pi^-$ reaction. Furthermore, the $pp \to \{pp\}_s\pi^0$ observables [25] are also well reproduced. However, the predictions for $A_{x,z}$ in Fig. 9(d) are radically different, especially between solution 2 and the other two. Hence even a low statistics measurement of this parameter would be sufficient to resolve some of the residual ambiguities. This would require the rotation of the proton polarization into the longitudinal direction, which could be achieved for a proton beam through the use of a Siberian snake. It is hoped that such an experiment will be carried out at ANKE [48] using the polarized deuterium target that was successfully commissioned in 2012. However, it should be noted that at the Indiana cyclotron a longitudinally polarized hydrogen target was achieved through the use of Helmholtz coils [49]. This approach would require significant extra development work at COSY.

Are there any theoretical indications as to which of the three solutions of Table I is to be preferred? Due to the strong coupling between the $^3S_1$ and $^3D_1$ partial waves, one cannot rely on using the Watson theorem to deduce the phases of

the M_p^S and M_p^D amplitudes. However, we would naively expect that the phases of the solutions that we have found should not differ drastically from the corresponding phases of elastic nucleon-nucleon scattering. It is interesting to note that the phases of the p-wave production amplitudes evaluated within χPT stay relatively close to the elastic phases, in spite of the coupled-channel dynamics [7]. It is important to note here that, although the Watson theorem suggests that the real production amplitude should acquire the elastic phase, one does not know if the "bare" amplitude is positive or negative. As a consequence there is a 180° ambiguity or, alternatively, it is only the tangent of the phase that is relevant.

Turning now to the results in Table I, one finds that $(\mathrm{Im}(M_p^S)/\mathrm{Re}(M_p^S), \mathrm{Im}(M_p^D)/\mathrm{Re}(M_p^D)) = (-0.44, -1.32)$, $(0.02, -0.48)$, and $(0.29, -0.53)$ for the three solutions. These are to be compared with the nucleon-nucleon phase-shift analysis values of $(\tan\delta_{^3S_1}, \tan\delta_{^3D_1}) = (0.03, -0.46)$ [33], and to the values from the theoretical analysis of $(0.04, -0.61)$ [7]. Although this theoretical calculation does not coincide exactly with the elastic phases, it is certainly much closer to solution 2 than solution 3. Specifically, the difference of 0.13 in $\tan\delta_{^3D_1}$ between theory and solution 2 corresponds to a phase difference of only 5°, whereas the difference for solution 3 is already 14°. There is therefore a distinct preference against solution 1 and possibly in favor of solution 2. However, it is difficult to quantify what emphasis should be placed on these theoretical arguments and a direct measurement of $A_{x,z}$ is required to clarify the situation.

We have made several assumptions in the partial wave fittings, especially by neglecting the interferences between the s and g waves and, more contentiously, between the p and f waves. Their inclusion within some model might change slightly the fit parameters in Table I. Nevertheless we believe that the solutions achieved are now sufficiently robust that they can be used in the framework of a modified chiral perturbation theory to achieve some of the goals outlined in the introduction.

ACKNOWLEDGMENTS

We are grateful to other members of the ANKE Collaboration for their help with this experiment and to the COSY crew for providing such good working conditions, especially of the polarized beam. The discussions with C. Hanhart on this problem over several years have been very illuminating. The work was supported by the COSY FFE program, STFC ST/J000159/1 grant, and the Shota Rustaveli National Science Foundation Grant No. 09-1024-4-200.

[1] S. Weinberg, Physica A **96**, 327 (1979).
[2] J. Gasser and H. Leutwyler, Ann. Phys. (NY) **158**, 142 (1984).
[3] C. Hanhart, U. van Kolck, and G. A. Miller, Phys. Rev. Lett. **85**, 2905 (2000).
[4] C. Hanhart and N. Kaiser, Phys. Rev. C **66**, 054005 (2002).
[5] V. Lensky *et al.*, Eur. Phys. J. A **27**, 37 (2006).
[6] A. A. Filin, V. Baru, E. Epelbaum, H. Krebs, C. Hanhart, A. E. Kudryavtsev, and F. Myhrer, Phys. Rev. C **85**, 054001 (2012).
[7] V. Baru, E. Epelbaum, J. Haidenbauer, C. Hanhart, A. E. Kudryavtsev, V. Lensky, and U.-G. Meißner, Phys. Rev. C **80**, 044003 (2009).
[8] A. Filin *et al.*, Phys. Lett. B **681**, 423 (2009).
[9] C. Hanhart, Phys. Rep. **397**, 155 (2004).
[10] E. Epelbaum, W. Glöckle, and U.-G. Meißner, Nucl. Phys. A **747**, 362 (2005).
[11] E. Epelbaum, A. Nogga, W. Glöckle, H. Kamada, Ulf-G. Meißner, and H. Witała, Phys. Rev. C **66**, 064001 (2002).
[12] T. S. Park *et al.*, Phys. Rev. C **67**, 055206 (2003).
[13] A. Gardestig and D. R. Phillips, Phys. Rev. Lett. **96**, 232301 (2006).
[14] D. Gazit, S. Quaglioni, and P. Navratil, Phys. Rev. Lett. **103**, 102502 (2009).
[15] V. A. Andreev *et al.* (MuSun Collaboration), PSI proposal R-08-01, arXiv:1004.1754.
[16] S. Ando, T. S. Park, K. Kubodera, and F. Myhrer, Phys. Lett. B **533**, 25 (2002)
[17] L. E. Marcucci, M. Piarulli, M. Viviani, L. Girlanda, A. Kievsky, S. Rosati, and R. Schiavilla, Phys. Rev. C **83**, 014002 (2011); L. E. Marcucci, A. Kievsky, S. Rosati, R. Schiavilla, and M. Viviani, Phys. Rev. Lett. **108**, 052502 (2012).
[18] J. Adam, Jr. *et al.*, Phys. Lett. B **709**, 93 (2012).
[19] L. E. Marcucci, R. Schiavilla, and M. Viviani, Phys. Rev. Lett. **110**, 192503 (2013).
[20] A. Gårdestig, D. R. Phillips, and C. Elster, Phys. Rev. C **73**, 024002 (2006).
[21] V. Lensky *et al.*, Eur. Phys. J. A **26**, 107 (2005).
[22] V. Lensky *et al.*, Eur. Phys. J. A **33**, 339 (2007).
[23] C. Ordonez and U. van Kolck, Phys. Lett. B **291**, 459 (1992).
[24] A. Kacharava, F. Rathmann, and C. Wilkin, COSY proposal 152, 2005, arXiv:nucl-ex/0511028.
[25] D. Tsirkov *et al.*, Phys. Lett. B **712**, 370 (2012).
[26] S. Dymov *et al.*, Phys. Lett. B **712**, 375 (2012).
[27] H. Hahn *et al.*, Phys. Rev. Lett. **82**, 2258 (1999).
[28] F. Duncan *et al.*, Phys. Rev. Lett. **80**, 4390 (1998).
[29] H. Hahn *et al.*, Phys. Rev. C **53**, 1074 (1996).
[30] E. Piasetzky, D. Ashery, M. A. Moinester, G. A. Miller, and A. Gal, Phys. Rev. Lett. **57**, 2135 (1986).
[31] R. Bilger *et al.*, Nucl. Phys. A **663**, 633 (2001).
[32] K. M. Watson, Phys. Rev. **88**, 1163 (1952); A. B. Migdal, Sov. Phys. JETP **1**, 2 (1955).
[33] R. A. Arndt, I. I. Strakovsky, and R. L. Workman, Phys. Rev. C **62**, 034005 (2000); R. A. Arndt, W. J. Briscoe, I. I. Strakovsky, and R. L. Workman, *ibid.* **76**, 025209 (2007); http://gwdac.phys.gwu.edu.
[34] R. Machleidt, K. Holinde, and Ch. Elster, Phys. Rep. **149**, 1 (1987); R. Machleidt, Phys. Rev. C **63**, 024001 (2001).
[35] J. Haidenbauer, K. Holinde, and M. B. Johnson, Phys. Rev. C **48**, 2190 (1993).
[36] V. Baru, E. Epelbaum, J. Haidenbauer, C. Hanhart, and V. Lensky (unpublished).
[37] S. Barsov *et al.*, Nucl. Instrum. Methods Phys. Res., Sect. A **462**, 364 (1997).
[38] B. Chiladze *et al.*, Part. Nuclei Lett. **113**(4), 95 (2002).
[39] S. Dymov *et al.*, Part. Nuclei Lett. **119**(2), 40 (2003).
[40] A. Khoukaz *et al.*, Eur. Phys. J. D **5**, 275 (1999).

[41] R. Schleichert *et al.*, IEEE Trans. Nucl. Sci. **50**, 301 (2003).
[42] M. Mikirtychyants *et al.*, Nucl. Instrum. Methods Phys. Res., Sect. A **721**, 83 (2013).
[43] D. Mchedlishvili *et al.*, Eur. Phys. J. A **49**, 49 (2013).
[44] H. J. Stein *et al.*, Atomic Energy **94**, 24 (2003); in Proceedings of the 18th Conference on Charged Particle Accelerators, RU-PAC 2002, NRCRF, Obninsk, 2004, edited by I. N. Meshkov, Vol. 1 (unpublished), p. 220, arXiv:1101.5963.
[45] R. A. Arndt, I. I. Strakovsky, R. L. Workman, and D. V. Bugg, Phys. Rev. C **48**, 1926 (1993).
[46] G. Riepe *et al.*, Nucl. Instrum. Methods Phys. Res., Sect. A **177**, 361 (1980).
[47] A. Gal, Few-Body Syst. **9**, 89 (1990).
[48] S. Dymov *et al.*, COSY proposal 213.1, 2013 (unpublished).
[49] T. Rinckel *et al.*, Nucl. Instrum. Methods Phys. Res., Sect. A **439**, 117 (2000).